Journal of ELECTRONIC MATERIALS, Vol. 47, No. 11, 2018
https://doi.org/10.1007/s11664-018-6602-1

Ternary $MoS_2/MoO_3/C$ Nanosheets as High-Performance Anode Materials for Lithium-Ion Batteries

JINLONG DU,[1,2] HONGDA WU,[1] XIAORONG WANG,[1] CHENGYUAN QI,[1] WEI MAO,[1] TIEQIANG REN,[1] QINGDONG QIAO,[1] and ZHANXU YANG[1,3,4]

1.—College of Chemistry, Chemical Engineering and Environmental Engineering, Liaoning Shihua University, Fushun 113001, Liaoning, People's Republic of China. 2.—North Huajin Chemical Industries Group Corporation, Panjin 124000, Liaoning, People's Republic of China. 3.—e-mail: zhanxuy@126.com. 4.—e-mail: yangzhanxu@lnpu.edu.cn

Ternary $MoS_2/MoO_3/C$ nanosheets were successfully synthesized via a chemical vapor deposition method. The hybrids were characterized by x-ray diffraction, scanning electron microscope, high-resolution transmission electron microscopy, raman and x-ray photoelectron spectroscopic methods. The as-obtained $MoS_2/MoO_3/C$ nanosheets applied as an anode material for lithium-ion batteries, showed high initial discharge/charge capacities at current rates of 0.5C, 1640.9 mA h g^{-1} and 1393.8 mA h g^{-1} respectively, with initial coulombic efficiency of approximately 84.9%. The material exhibited superior rate capabilities, with specific discharge capacities of 1240.2 mA h g^{-1}, 1048.5 mA h g^{-1}, 917.2 mA h g^{-1}, 742.3 mA h g^{-1}, 663.6 mA h g^{-1}, 601.8 mA h g^{-1} and 593.4 mA h g^{-1} at current rates of 0.2C, 0.4C, 1C, 4C, 8C, 12C and 15C, respectively. This superior electrochemical performance was mainly due to the uniformly-distributed MoS_2 nanosheets and to highly graphitized carbon, which not only mitigated mechanical stress during repeated cycling, but also provided good conductivity.

Key words: MoS_2, MoO_3, carbon, nanosheets, lithium-ion battery

INTRODUCTION

Two-dimensional layered molybdenum disulfide (MoS_2) has been a research focus in the fields of lubricants,[1] transistors,[2,3] and supercapacitors,[4,5] etc. The individual S-Mo-S layers formed by strong ionic/covalent forces between Mo and S atoms are stacked through weak van der waals interactions.[6,7] Owing to the weak van der Waals interactions between MoS_2 layers,[8–12] the hierarchical MoS_2 particles allow for insertion and extraction of Li ions without remarkable volume damage. However, fast structural deterioration during the cycling process and poor electrical/ionic conductivity of MoS_2 have been found to result in unsatisfactory cycling performance and low rate capability, thus failing to meet the requirements for commercial use in lithium-ion battery (LIB) applications.

(Received October 28, 2017; accepted August 10, 2018; published online August 21, 2018)

In order to circumvent these obstacles, two major strategies are currently developed for the modification of MoS_2: (1) decreasing the characteristic dimensions of MoS_2, controlling morphologies such as nanoflowers,[13] nanospheres[14–17] and nanosheets[18,19]; (2) constructing a conductive and robust scaffold to form combinations, such as few-layered MoS_2 grown on carbon nanosheets,[20] monolayer MoS_2 embedded in the carbon nanofibers,[21,22] and ultrathin MoS_2 nanosheets on nitrogen-doped graphene nanosheets[23,24] or N-doped carbon nanoboxes.[25] In pursuing the first strategy, although the performance has been significantly improved, conductivity still remains poor. As to the second strategy, the combination of MoS_2 and carbon solves the problem of conductivity. However, this simple compound is susceptible to stacking and reuniting during the charge and discharge circulation process thus leading to loss of capacity when used as LIB anode material. Therefore, developing an environmentally-friendly, facile and scalable route is still a challenge.

In this work, we have synthesized ternary MoS_2/MoO_3/C nanosheets by a simple chemical vapor deposition (CVD) method. The uniqueness of this method lies in that it inserts organic amine into a MoO_3 interlayer as a precursor, and then obtains the final products through an in situ transformation method. This structure is not as simple as that of most composite materials. Due to vapor phase vulcanization, the MoO_3 layer outside the MoO_3/C motherboard is mostly vulcanized, while the MoO_3 layer inside is vulcanized by only a small amount. Thus, mixed ternary MoS_2/MoO_3/C nanosheets are formed in situ from binary MoO_3/C nanosheets. The nanosheets can greatly facilitate the transportation of Li^+ and electrons. Meanwhile, the high surface area of the nanosheets allows extensive contact between the electrode and the electrolyte, thus providing good conditions for lithium and electron diffusion. More importantly, the optimized MoS_2/MoO_3/C nanosheets exhibit high reversible capacity, as well as good cycling stability and high-rate capability as anode materials for LIBs (Scheme 1).

RESULTS AND DISCUSSION

The crystallinity of the as-prepared ternary MoS_2/MoO_3/C nanosheets and MoO_3/C is revealed by x-ray diffraction (XRD), shown in Fig. 1a. The diffraction profiles demonstrate the phase purity of MoS_2 with crystallized hexagonal structure (JCPDS 37-1492). MoS_2/MoO_3/C nanosheets show conspicuous peaks at 33.02° and 58.64°, which are indexed to the (100) and (110) planes of crystalline MoS_2 , respectively.[26–28] A sharp peak at 9.76° (marked by #1) and a low sharp peak at 16.54° (marked by #2) can be observed in the composites, attributable to the distance of adjacent MoS_2 nanosheets in amorphous carbon and the distance between the carbon layer and the MoS_2 layer, respectively.[26,27,29,30] Therefore, the XRD pattern shows that no significant (002) crystal face of MoS_2 or diffraction peaks of carbon are observed in the final product. From the MoO_3/C curve, we can observe that the diffraction peak of (010) is the interpolated peak of the precursor at about 5.35°, which indicates that dodecylamine has been successfully intercalated between MoO_3 layers, according to the literature.[31,32] Subsequently, the interlamellar spacing gradually shrinks owing to the decomposition of intercalated dodecylamine. Therefore, the (010) diffraction peaks move to a high angle.

The MoS_2/MoO_3/C composite exhibits a 2D nanosheet-shaped morphology with a few micrometers, according to the scanning electron microscope (SEM) image of sample (Fig. 1b). From the

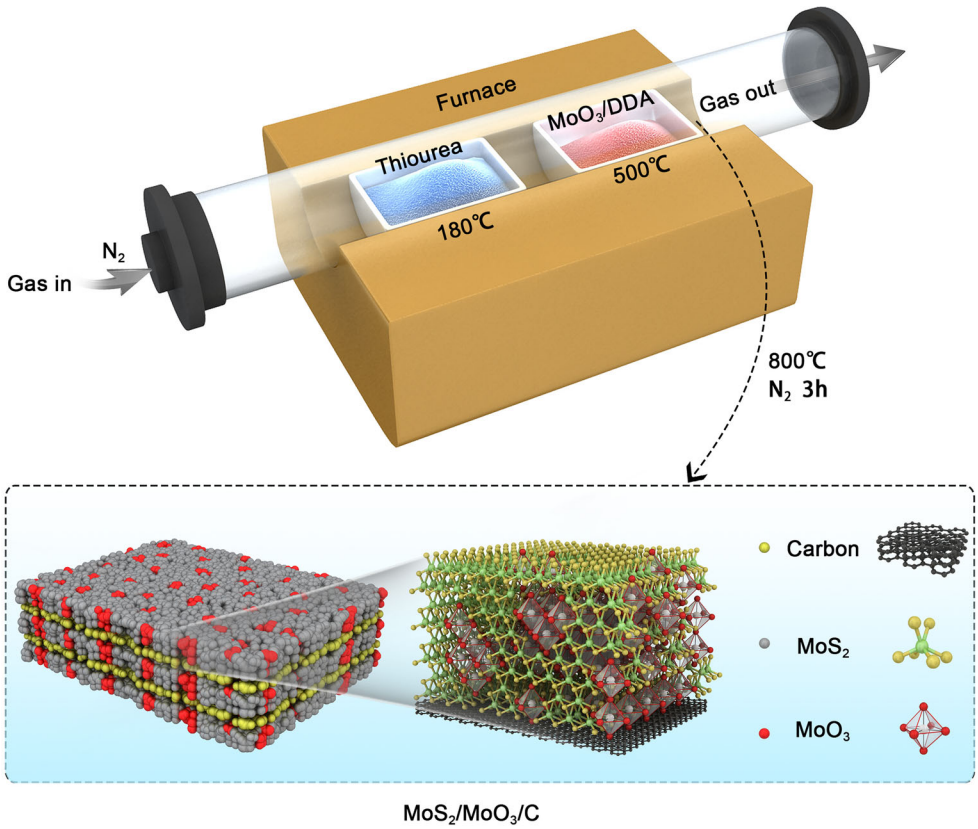

Scheme 1. Schematic of the synthesis process of ternary MoS_2/MoO_3/C nanosheets.

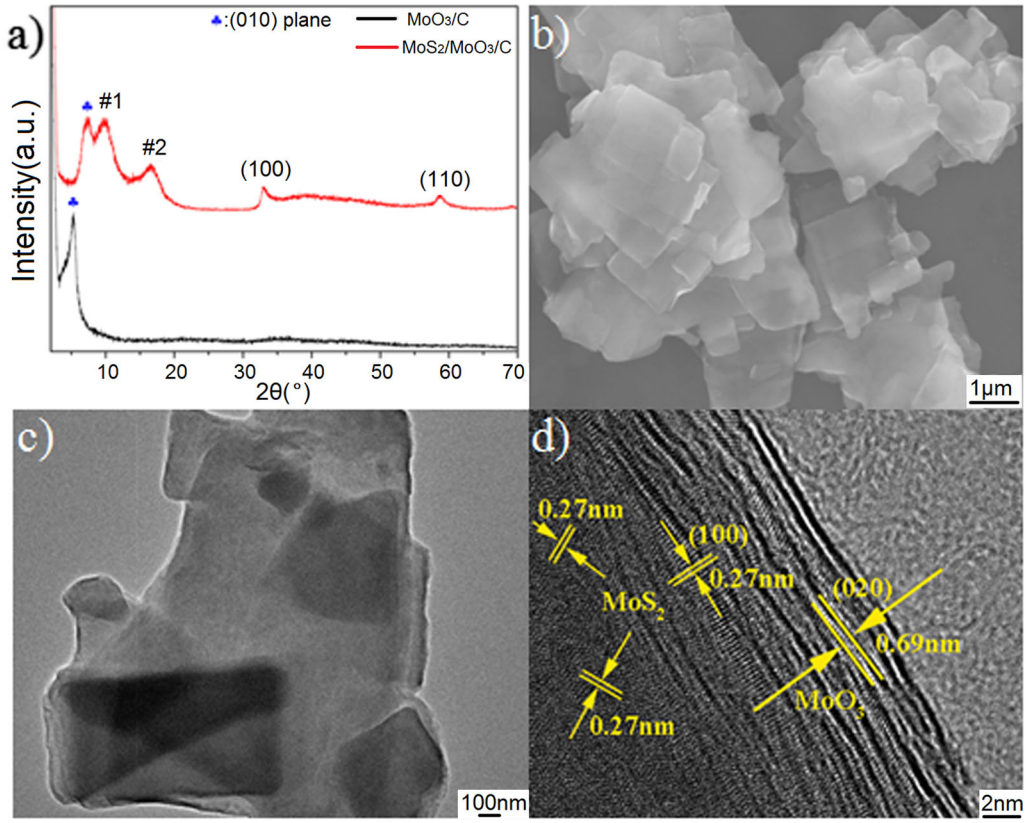

Fig. 1. (a) The XRD patterns of $MoS_2/MoO_3/C$ nanosheets; (b) SEM image of the surface of sample $MoS_2/MoO_3/C$; (c) the TEM image of $MoS_2/MoO_3/C$; (d) high-resolution TEM images of $MoS_2/MoO_3/C$.

transmission electron microscope (TEM) image (Fig. 1c) we can also clearly observe the nanosheet structure. Furthermore, the high-resolution transmission electron microscopy (HRTEM) image (Fig. 1d) of $MoS_2/MoO_3/C$ validates the presence of MoS_2 and MoO_3 nanosheets. It can be seen from the figure that the edge of the nanosheet is made up of lattice fringes (0.69 nm) of MoO_3, and the interior is all made up of MoS_2 lattice stripes (0.27 nm) corresponding to the (100) lattice plane; this is consistent with the XRD analysis results. In general, the synthesis of nanosheets by the precursor MoO_3 nanosheets and the sulfur source in situ reaction leads to the uniqueness of this material.

A Raman test (Fig. 2a) was performed to further investigate the $MoS_2/MoO_3/C$ nanosheets. The Raman spectrum of this product exhibits obvious peaks at 283.63 cm^{-1}, 821.36 cm^{-1} and 994.7 cm^{-1} in the wave number range of 200 to 1800 cm^{-1}, which are in agreement with the reported Raman spectra of α-MoO_3.[33–36] Furthermore, the first order in-plane phonon vibration mode (E^1_{2g}) and out-of-plane vibration mode (A_{1g}) of MoS_2 appear at the wavenumbers of 378.69 cm^{-1} and 401.04 cm^{-1}, respectively.[24,37,38] The energy difference between the two Raman peaks (Δk) can be used to determine the number of layers in few-layer MoS_2 crystals.[39] The Δk is about 22.35 cm^{-1}(inset in Fig. 2a), indicating the MoS_2 crystals in the hybrids are composed of few-layer MoS_2 nanosheets. In addition to the typical peaks for MoO_3 and MoS_2 materials, the other two distinct peaks around the D band (1363.85 cm^{-1}) and G band (1578.21 cm^{-1}) demonstrate the existence of carbon. The fitting of D and G peaks can be obtained with an I_D/I_G intensity ratio of 1.07, suggesting a relatively better graphitization.[20,27]

The signals of Mo, S, O and C are observed, respectively, in the x-ray photoelectron spectroscopic (XPS) images (Fig. 2b), further confirming the presence of molybdenum sulfide, molybdenum oxide and C. Figure 2c shows the high resolution spectrum of Mo. The two main components (Mo^{IV} $3d_{5/2}$ (229.2 eV) and Mo^{IV} $3d_{3/2}$ (232.2 eV) are the characteristics of MoS_2,[20,40,41] while the small shoulder peak at around 226.5 eV is identified as S 2 s.[42] The presence of the other two XPS peaks, Mo^{VI} $3d_{5/2}$ (232.6 eV) and Mo^{VI} $3d_{3/2}$ (235.6 eV) indicates the incomplete reaction of MoO_3.[43–45] The binding energies at 162.1 eV and 163.3 eV in the S 2p spectrum are attributed to S^{2-} of MoS_2 (Fig. 2 d).[14,23] The O 1s XPS spectrum shows that the binding energy of O 1s is 531.6 eV (Fig. 2e), which can be assigned to O^{2-} in MoO_3.[35,46] Figure 2f exhibits the C1s XPS peak centered at 284.2 eV, which is attributed to the binding energy of the sp^2

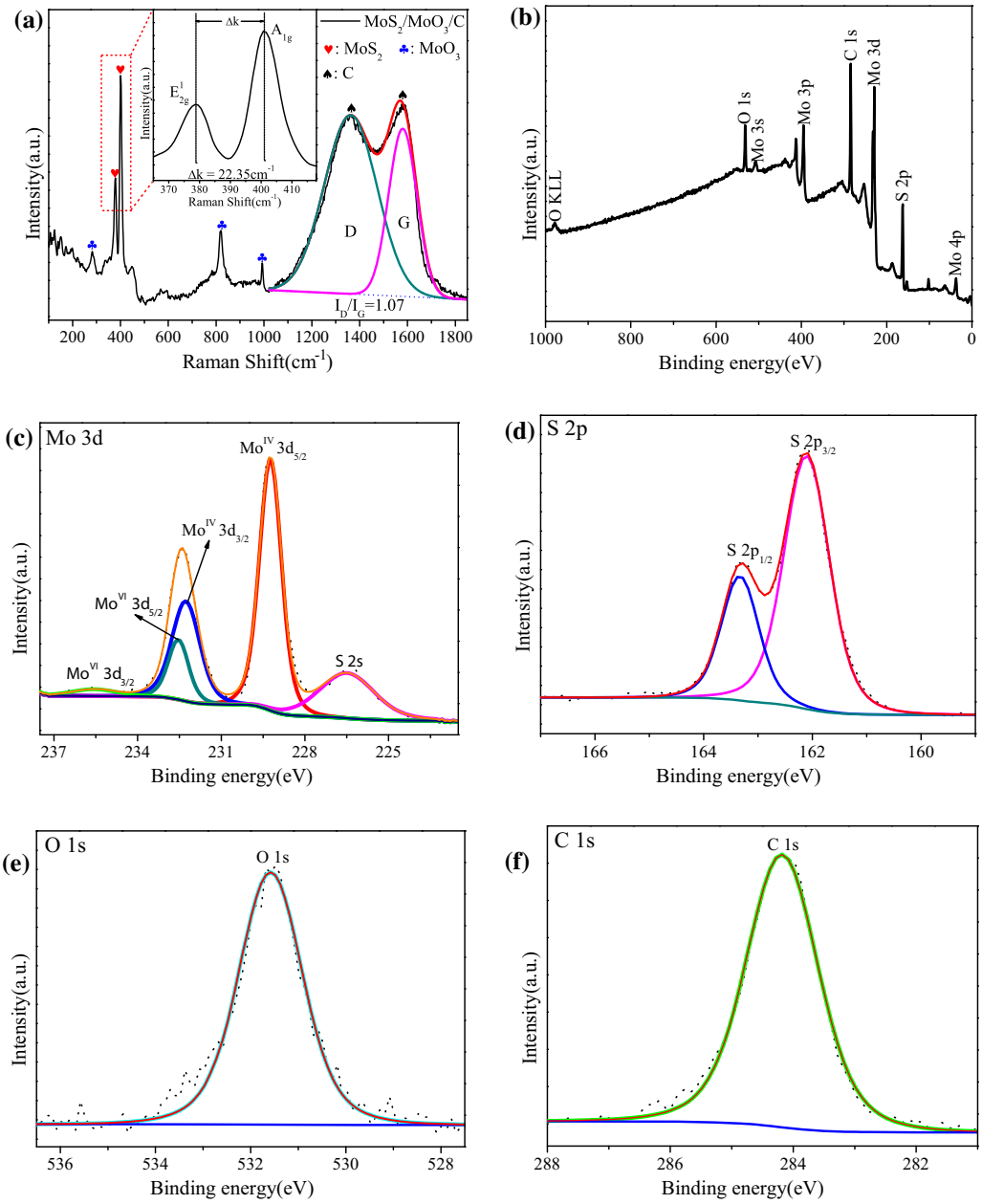

Fig. 2. (a) Raman spectra of the $MoS_2/MoO_3/C$ nanosheets. The inset of (a) shows the enlargement at the red mark in the figure; (b) XPS survey spectrum of the $MoS_2/MoO_3/C$ nanosheets and the corresponding high-resolution XPS scans of (c) Mo 3d, (d) S 2p, (e) O 1s, (f) C 1s.

C–C bond.[47,48] This further verifies the existence of amorphous carbon composites.

Subsequently, the ternary $MoS_2/MoO_3/C$ nanosheets were investigated as an anode material for LIBs. The long-term cycling performance of the obtained materials was evaluated through discharge/charge at a current rate of 0.5C (0.43 A g^{-1}) (Fig. 3a). As shown in the charge/discharge curves of the $MoS_2/MoO_3/C$ nanosheets electrode, the initial discharge and charge capacities are about 1640.9 mAh g^{-1} and 1393.8 mAh g^{-1}, respectively. The initial discharge and charge capacities of the MoO_3/C are about 1115.9 mAh g^{-1} and 829.8 mAh g^{-1}, respectively. The initial discharge and charge capacities of the commercial MoS_2 are about 1025.4 mAh g^{-1} and 672.6 mAh g^{-1}, respectively. The coulombic efficiency is about 84.9%, significantly higher than that of commercial MoO_3/C (74.4%) and MoS_2 (65.6%). The specific reversible capacity of the $MoS_2/MoO_3/C$ nanosheets in the 20th cycle slightly decreases, owing to the reversible growth of solid electrolyte interface (SEI) film on the surface of the electrodes, the incomplete wetting of the internal portion of electrode and dissolution of the intermediate products (polysulfide) in the electrolyte.[14,49]

With the increase of the cycle number, the capacity is about 961.4 mAh g^{-1}, indicating that the material has good stability. The rate capacities display highly reversible storage properties as well as high cycling performance. As shown in Fig. 3b, the hybrid $MoS_2/MoO_3/C$ nanosheets deliver reversible capacities of 1240.2 mA h g^{-1}, 1048.5 mA h g^{-1}, 917.2 mA h g^{-1}, 794.9 mA h g^{-1}, 742.3 mA h g^{-1}, 663.6 mA h g^{-1}, 628.7 mA h g^{-1}, 601.8 mA h g^{-1} and 593.4 mA h g^{-1} at current rates of 0.2C (0.22 A g^{-1}), 0.4C (0.44 A g^{-1}), 1C (0.89 A g^{-1}), 2C (1.78 A g^{-1}), 4C (2.68 A g^{-1}), 8C (4.46 A g^{-1}), 10C (6.25 A g^{-1}), 12C (7.14 A g^{-1}) and 15C (8.04 A g^{-1}), respectively. If the current rate is dropped to 0.2C after cycling at 15C, the capacity of the anode gradually recovers to 1091.9 mAh g^{-1}, suggesting good reversibility of the materials. The excellent electrochemical performance of $MoS_2/MoO_3/C$ nanosheets can be attributed to the following factors: (1) The structure of the nanosheets has much open space and a large specific surface area, which can afford a large number of reaction sites. Thus, the $MoS_2/MoO_3/C$ nanosheets show a high specific capacitance. (2) The unique in-situ composite structure of MoS_2 and MoO_3 can reduce aggregation during the lithiation/delithiation process thus enabling us to obtain excellent cycling and rate performance. (3) The insertion of carbon not only improves the conductivity of the electrode material, but also enhances the structural stability.

In order to further study the mechanism of the material's cycle performance, cyclic voltammetry was conducted for $MoS_2/MoO_3/C$, as shown in Fig. 3c. During the first cycle, two reduction peaks (0.67 V and 0.45 V) and one corresponding oxidation peak (2.4 V) are observed. The peak (#1) at 0.67 V can be assigned to the intercalation of Li ion into MoS_2 interlayer to form Li_xMoS_2, and the other peak at 0.45 V(#2) is related to the reduction of MoS_2 into Mo metal particles embedded into a Li_2S matrix ($MoS_2 + 4Li \rightarrow Mo + 2Li_2S$) and the formation of SEI layers.[50,51] For the charging process, the peak (#3) at 2.33 V can be clearly identified for the first and subsequent cycles, which is attributed to the delithiation of Li_2S to sulfur ($Li_2S \rightarrow 2Li^+ + S + 2e^-$).[52] In the following two cathodic scans, different discharge profiles are obtained with four peaks observed at 1.75 V, 1.02 V, 0.39 V and 2.40 V, respectively, which might be due to the following three reactions: $2Li^+ + S + 2e \rightarrow Li_2S$, $MoS_2 + xLi^+ + xe \rightarrow Li_xMoS_2$, $Li_xMoS_2 + (4-x)Li^+ + (4-x)e \rightarrow Mo + 2Li_2S$ and $Li_2S - 2e^- \rightarrow 2Li^+ + S$. The CV curves of the second and third cycles are almost overlapped, indicating that the electrode may have good cycling performance.

The electrochemical impedance spectra (EIS) of the $MoS_2/MoO_3/C$ nanosheets electrode were

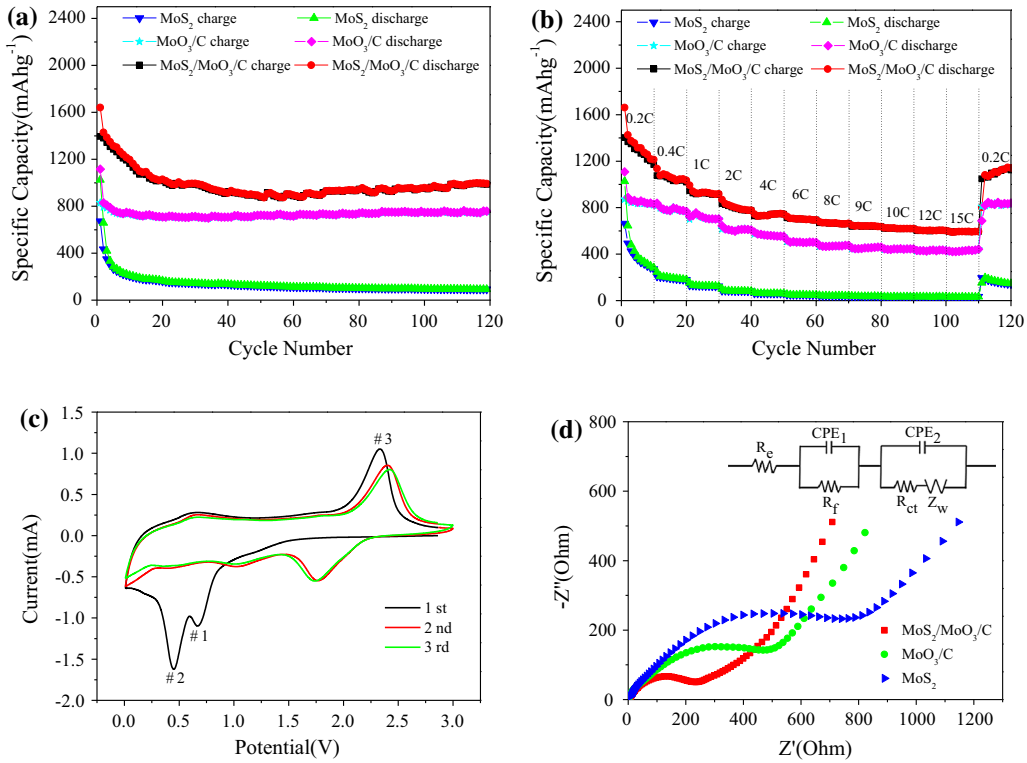

Fig. 3. (a) Cycle ability tests on MoS_2 and $MoS_2/MoO_3/C$ nanosheets at 0.5C; (b) The rate performance of MoS_2 and $MoS_2/MoO_3/C$ at different current rates from 0.2–15C; (c) Cyclic voltammetry curves under a scanning rate of 0.3 mV s^{-1} of $MoS_2/MoO_3/C$; (d) EIS spectra of as-prepared MoS_2, MoO_3/C and $MoS_2/MoO_3/C$ samples.

investigated after three discharge/charge cycles in the frequency range from 100 kHz to 0.01 Hz (Fig. 3d). The curve of the Nyquist-fitting for getting the equivalent circuit is given in the inset. R_e is the internal resistance of the battery, R_f represents the SEI membrane resistance, CPE_1 and CPE_2 stands for constant phase elements, R_{ct} represents the faradic charge-transfer resistance and the Warburg impedance Z_w reflects the solid state diffusion in the equivalent circuit. The semicircle in the high-frequency region could be ascribed to the constant phase element of the SEI layer and contact resistance. The inclined line was attributed to Warburg impedance corresponding to the lithium-diffusion process.[53] By fitting the equivalent circuit, the charge transfer resistances (R_{ct}) of MoS_2, MoO_3/C and MoS_2/MoO_3/C were 782.5 Ω, 467.7 Ω and 124.3 Ω, respectively. It could be seen that MoS_2/MoO_3/C has a low charge-transfer resistance. It is also clear from the curve that MoS_2/MoO_3/C has a smaller semicircular diameter at high frequencies. The Warburg slope of MoS_2/MoO_3/C is higher than that of MoO_3/C and commercial MoS_2, further indicating faster ion diffusion in MoS_2/MoO_3/C electrode. These results confirm that the ternary MoS_2/MoO_3/C nanosheets have distinctively improved the electronic conductivity of the hybrid.

CONCLUSIONS

In summary, ternary MoS_2/MoO_3/C nanosheets have been successfully synthesized via a simple method. The composites could exhibit excellent cyclic capacity (961.4 mAh g^{-1} at 0.5C), and outstanding rate performance (remained 593.4 mAh g^{-1} at a high rate of 20C) as a result of their unique structure with mixed MoS_2/MoO_3/C nanosheets and uniformly dispersed C for high conductivity. This work provides a novel and facile way for design of a composite with multiple phase nanosheets.

METHODS

Characterization

X-ray powder diffraction (XRD) measurements were obtained on a Bruker D8 Advance diffractometer operated at 40 kV and 40 mA in the range of 1.5–70° with Cu-Ka radiation (λ = 0.15406 nm). The particle morphologies of the products were observed by means of a field emission scanning electron microscope (FESEM) (Hitachi SU 8010) operated at an acceleration voltage of 15 kV. High-resolution transmission electron microscopy (HRTEM) was performed on a JEM-2100 microscope (JEOL). Raman spectra were recorded on a DXR raman microscope (Thermo Scientific) with a 532 nm excitation laser (setting 3 mW power, 10 s exposure time, and 20 accumulations). X-ray photoelectron spectroscopic (XPS) measurement of the composites was conducted on an ESCALAB 250 spectrometer (Thermo Fisher Scientific) with an Al Ka (1486.6 eV) x-ray source operated at 15 kV and 150 mW.

Electrochemical Measurements

The working electrodes were made by coating a paste of active materials, Super P, and binder (polyvinylidene fluoride, PVDF) in a weight ratio of 80: 10: 10 on a copper-foil collector. The active mass loading of about 0.8 mg cm^{-2} was employed in this work. The electrode film was subjected to a roll press and electrodes of 10 mm diameter were punched out. The negative electrodes were dried at 100°C for 12 h in a vacuum oven. Cointype cells (CR 2032) were assembled in an argon-filled glove box with an electrolyte of 1 mol L^{-1} $LiPF_6$ in EC-EMC-DMC (1:1:1 volume ratio) solution and a separator of Celgard 2400. The electrochemical data were collected using a LAND CT2001A test system within the potential range of 0.01–3.0 V (versus Li/Li^+). The assembly of the cell was conducted in an Ar-filled glove-box followed by overnight aging treatment before the test. Cycling voltammetry (CV) was measured at a scan rate of 0.5 mV s^{-1}using a CHI 660C electrochemical workstation (Shanghai CHI Instruments). Electrochemical impedance spectroscopy (EIS) was performed in the frequency range of 0.01–10^5 Hz on the PARSTAT 2273 electrochemical workstation (Ametek).

EXPERIMENTAL

Synthesis of the Ternary MoS_2/MoO_3/C Nanosheets

The ternary MoS_2/MoO_3/C nanosheets were synthesized by a chemical vapor deposition (CVD) method. In a typical experiment, the nanocomposites were prepared by adding 15 mL dodecylamine into 170 mL anhydrous ethanol, followed by stirring until the samples were dissolved. Subsequently, 1.71 g MoO_3 was added into the mother solution and the mixture was heated at a temperature of 70°C for 24 h. Then, it was filtered and washed with anhydrous ethanol. After being dried at 70°C for 24 h, the as-obtained white powder samples were the desired precursor composites. The as-prepared composite (0.2 g) was placed in the high temperature area of a vacuum pipe furnace for chemical vapor deposition, and an appropriate amount thiourea was placed in the low temperature area. The sample was heated to 500°C at a heating rate of 1°C min^{-1} under N_2 gas, and the sulfur source was heated to 180°C at a heating rate of 3°C min^{-1}, both were heated for 3 h after reaching the highest point. They were further heated up to 800°C for 3 h at a heating rate of 3°C min^{-1} following vulcanization. The obtained sample was denoted as MoS_2/MoO_3/C.

For comparison, pure MoO_3/C was prepared under the same conditions but without assistance of thiourea.

ACKNOWLEDGEMENTS

This study was supported by the National Natural Science Foundation of China (21671092), the Program for Liaoning Excellent Talents in University (LNET LR2015036), Research Fund Project for the Construction of Instrument and Equipment Sharing Service Platform of Liaoning Province (2016LD0106) and the Opening Funds of State Key Lab of Chemical Resource Engineering.

CONFLICT OF INTEREST

The authors declare no competing financial interest.

REFERENCES

1. Z. Chen, X. Liu, Y. Liu, S. Gunsel, and J. Luo, *Sci. Rep.* 5, 12869 (2015).
2. R. Kappera, D. Voiry, S.E. Yalcin, B. Branch, G. Gupta, and M. Chhowalla, *Nat. Mater.* 13, 1128 (2014).
3. D.J. Late, Y.K. Huang, B. Liu, J. Acharya, J. Luo, A. Yan, and D. Charles, *ACS Nano* 7, 4879 (2013).
4. M.A. Bissett, I.A. Kinloch, and R.A.W. Dryfe, *ACS Appl. Mater. Interfaces* 7, 17388 (2015).
5. M. Acerce, D. Voiry, and M. Chhowalla, *Nat. Nanotechnol.* 10, 313 (2015).
6. J. Zhang, J.M. Soon, K.P. Loh, J. Yin, and J. Ding, *Nano Lett.* 7, 2370 (2007).
7. S.W. Han, H. Kwon, S.K. Kim, S. Ryu, W.S. Yun, D.H. Kim, J.H. Hwang, J.-S. Kang, J. Baik, H.J. Shin, and S.C. Hong, *Phys. Rev. B* 84, 045409 (2011).
8. G. Du, Z. Guo, S. Wang, R. Zeng, and Z. Chen, *Chem. Commun.* 46, 1106 (2010).
9. C. Feng, J. Ma, H. Li, R. Zeng, Z. Guo, and H. Liu, *Mater. Res. Bull.* 44, 1811 (2009).
10. T. Stephenson, Z. Li, B. Olsen, and D. Mitlin, *Energy Environ. Sci.* 7, 209 (2014).
11. H. Wang, D. Ren, Z. Zhu, P. Saha, H. Jiang, and C. Li, *Chem. Eng. J.* 288, 179 (2016).
12. J. Xiao, D. Choi, L. Cosimbescu, P. Koech, J. Liu, and J.P. Lemmon, *Chem. Mater.* 22, 4522 (2010).
13. Z. Hu, L. Wang, K. Zhang, J. Wang, F. Cheng, Z. Tao, and J. Chen, *Angew. Chem. Int. Ed. Engl.* 53, 12794 (2014).
14. S. Zhang, B.V.R. Chowdari, Z. Wen, J. Jin, and J. Yang, *ACS Nano* 9, 12464 (2015).
15. S.K. Park, S.H. Yu, S. Woo, J. Ha, J. Shin, Y.E. Sung, and Y. Piao, *CrystEngComm* 14, 8323 (2012).
16. M. Wang, G. Li, H. Xu, Y. Qian, and J. Yang, *ACS Appl. Mater. Interfaces* 5, 1003 (2013).
17. Y. Zhang, Y. Li, H. Li, F. Yin, Y. Zhao, and Z. Bakenov, *J. Nanopart. Res.* 18, 1 (2016).
18. T. Yang, Y. Chen, B. Qu, L. Mei, D. Lei, H. Zhang, and Q. Li, *Electrochim. Acta* 115, 165 (2014).
19. S. Zhang, X. Yu, H. Yu, Y. Chen, P. Gao, C. Li, and C. Zhu, *ACS Appl. Mater. Interfaces* 6, 21880 (2014).
20. J. Zhou, J. Qin, X. Zhang, C. Shi, E. Liu, N. Zhao, and C. He, *ACS Nano* 9, 3837 (2015).
21. C. Zhao, J. Kong, X. Yao, X. Tang, Y. Dong, and X. Lu, *ACS Appl. Mater. Interfaces* 6, 6392 (2014).
22. C. Zhu, X. Mu, P.A. Aken, Y. Yu, and J. Maier, *Angew. Chem. Int. Ed. Engl.* 53, 2152 (2014).
23. K. Chang, D. Geng, X. Li, J. Yang, Y. Tang, M. Cai, R. Li, and X. Sun, *Adv. Energy Mater.* 3, 839 (2013).
24. J.M. Jeong, K.G. Lee, S. Chang, J.W. Kim, Y. Han, S.J. Lee, and B.G. Choi, *Nanoscale* 7, 324 (2015).
25. X. Yu, H. Hu, Y. Wang, H. Chen, and X.W. Lou, *Angew. Chem. Int. Ed. Engl.* 54, 7395 (2015).
26. K. Chang, W. Chen, L. Ma, H. Li, F. Huang, Q. Zhang, and J. Lee, *J. Mater. Chem.* 21, 6251 (2011).
27. H. Jiang, D. Ren, H. Wang, Y. Hu, S. Guo, H. Yuan, P. Hu, L. Zhang, and C. Li, *Adv. Mater.* 27, 3687 (2015).
28. J. Wang, C. Luo, T. Gao, A. Langrock, A.C. Mignerey, and C. Wang, *Small* 11, 473 (2015).
29. K. Chang and W. Chen, *J. Mater. Chem.* 21, 17175 (2011).
30. G. Huang, T. Chen, W. Chen, Z. Wang, K. Chang, L. Ma, F. Huang, D. Chen, and J.Y. Lee, *Small* 9, 3693 (2013).
31. Y. Jing, Q. Pan, Z. Cheng, X. Dong, and Y. Xiang, *Mater. Sci. Eng. B* 138, 55 (2007).
32. J. Qiu, Z. Yang, and Y. Li, *J. Mater. Chem. A* 3, 24245 (2015).
33. D.E. Diaz-Droguett, R.E. Far, V.M. Fuenzalida, and A.L. Cabrera, *Mater. Chem. Phys.* 134, 631 (2012).
34. J.Z. Ou, J.L. Campbell, D. Yao, W. Wlodarski, and K. Kalantar-zadeh, *J. Phys. Chem. C* 115, 10757 (2011).
35. T. Wang, J. Li, and G. Zhao, *Powder Technol.* 253, 347 (2014).
36. D.D. Yao, J.Z. Ou, K. Latham, S. Zhuiykov, A.P. O'Mullane, and K. Kalantar-zadeh, *Cryst. Growth Des.* 12, 1865 (2012).
37. H. Li, Q. Zhang, C.C.R. Yap, B.K. Tay, T.H.T. Edwin, A. Olivier, and D. Baillargeat, *Adv. Funct. Mater.* 22, 1385 (2012).
38. J. Shao, T. Gao, Q. Qu, Q. Shi, Z. Zuo, and H. Zheng, *J. Power Sources* 324, 1 (2016).
39. Y. Yu, C. Li, Y. Liu, L. Su, Y. Zhang, and L. Cao, *Sci. Rep.* 3, 1866 (2013).
40. X. Geng, W. Wu, N. Li, W. Sun, J. Armstrong, A. Al-hilo, M. Brozak, J. Cui, and T. Chen, *Adv. Funct. Mater.* 24, 6123 (2014).
41. X. Wang, G. Li, M.H. Seo, F.M. Hassan, M.A. Hoque, and Z. Chen, *Adv. Energy Mater.* 5, 1501106 (2015).
42. X. Wang, Y. Zhang, and Z. Chen, *Mater. Res. Express* 3, 065014 (2016).
43. Z. Chen, D. Cummins, B.N. Reinecke, E. Clark, M.K. Sunkara, and T.F. Jaramillo, *Nano Lett.* 11, 4168 (2011).
44. B. Li, S. Yang, N. Huo, Y. Li, J. Yang, R. Li, C. Fan, and F. Lu, *RSC Adv.* 4, 26407 (2014).
45. Z. Yin, X. Zhang, Y. Cai, J. Chen, J.I. Wong, Y. Tay, J. Chai, J. Wu, Z. Zeng, B. Zheng, H.Y. Yang, and H. Zhang, *Angew. Chem. Int. Ed. Engl.* 53, 12560 (2014).
46. X. Wang and Y. Zhang, *Philos. Mag. Lett.* 96, 347 (2016).
47. S.H. Choi and Y.C. Kang, *Nano Res.* 8, 2492 (2015).
48. Y. Zhang, L. Zuo, Y. Huang, L. Zhang, F. Lai, W. Fan, and T. Liu, *ACS Sustain. Chem. Eng.* 3, 3140 (2015).
49. Y. Xia, B. Wang, X. Zhao, G. Wang, and H. Wang, *Electrochim. Acta* 187, 55 (2016).
50. D. Ren, H. Jiang, Y. Hu, L. Zhang, and C. Li, *RSC Adv.* 4, 40368 (2014).
51. Z. Wang, T. Chen, W. Chen, K. Chang, L. Ma, G. Huang, D. Chen, and J.Y. Lee, *J. Mater. Chem. A* 1, 2202 (2013).
52. Q. Qu, F. Qian, S. Yang, T. Gao, W. Liu, J. Shao, and H. Zheng, *ACS Appl. Mater. Interfaces* 8, 1398 (2016).
53. G. Chen, S. Wang, R. Yi, L. Tan, H. Li, M. Zhou, L. Yan, Y. Jiang, S. Tan, D. Wang, S. Deng, X. Meng, and H. Luo, *J. Mater. Chem. A* 4, 9653 (2016).